

A method for 3-D hydraulic fracturing simulation

S. Secchi · B. A. Schrefler

Received: 15 February 2012 / Accepted: 14 June 2012
© Springer Science+Business Media B.V. 2012

Abstract We present a method for the simulation of 3-D hydraulic fracturing in fully saturated porous media. The discrete fracture(s) is driven by the fluid pressure. A cohesive fracture model is adopted where the fracture follows the face of the elements around the fracture tip which is closest to the normal direction of the maximum principal stress at the fracture tip. No predetermined fracture path is needed. This requires continuous updating of the mesh around the crack tip to take into account the evolving geometry. The updating of the mesh is obtained by means of an efficient mesh generator based on Delaunay tessellation. The governing equations are written in the framework of porous media mechanics theory and are solved numerically in a fully coupled manner. An examples dealing with a concrete dam is shown.

Keywords Hydraulic fracturing · Cohesive fracture model · 3D finite element solution

1 Introduction

Fluid-driven fracture propagating in geomaterials such as rocks, soil or concrete are encountered in many engineering problems. Hydraulic fracturing is used to enhance the recovery of hydrocarbons from underground reservoirs and most recently for extracting gas and oil from shales (TAMEST 2011). This is an emerging field where the consequences on the environment have still to be assessed. On the other hand, the reserves of shale gas both in the United States (estimated around 70 tr m^3) and in a lesser measure in Europe (estimated 14 tr m^3) are enormous and justify the interest on modelling of hydraulic fracturing. Another application of importance is related to the overtopping stability analysis of dams.

Contributions to the mathematical modelling of fluid-driven fractures have been made continuously since the 1960s, beginning with Perkins and Kern (1964). These authors made various simplifying assumptions, for instance regarding fluid flow, fracture shape and leakage velocity from the fracture. Among other contributions, reference can be made to Rice and Cleary (1976), Cleary (1978), Huang and Russel (1985a), Huang and Russel (1985b) and Detournay and Cheng (1991). All these contributions present analytical solutions, in the frame of linear fracture mechanics assuming the problem to be stationary. Further, they suffer the limits of the analytical approach, in particular the inability to represent an evolutionary problem in a domain with a real complexity. Other papers deal

S. Secchi
CNR, ISIB, Corso Stati Uniti 4, 35127 Padua, Italy

B. A. Schrefler (✉)
Department of Civil, Environmental and Architectural
Engineering, University of Padova, Via Marzolo 9,
35131 Padua, Italy
e-mail: bas@dic.unipd.it

with the analysis of solid and fluid behaviour near the crack tip (Advani et al. 1997; Garagash and Detournay 2000). A general model has been presented by Boone and Ingraffea (1990) in the context of linear fracture mechanics. It allows for fluid leakage in the medium surrounding the fracture and assumes a moving crack depending on the applied loads and material properties. Hence, fracture length is a natural product of the solution algorithm, not the result of previous assumptions. A finite element/difference solution is adopted in this case. Carter et al. (2000) put forward a fully 3-D hydraulic fracture model which relies on hypotheses similar to Boone and Ingraffea (1990), in particular assuming the positions where fractures initiate, but completely neglects the fluid continuity equation in the medium surrounding the fracture. Schrefler et al. (2006) and Secchi et al. (2007) presented a two dimensional cohesive fracture model in a fully saturated porous medium where remeshing is used to follow the advancing fracture and the above listed limiting assumptions have been eliminated. Finally Réthoré et al. (2008) used the Extended Finite Element Method for 2-D hydraulic fracturing simulation.

As far as numerical fracture analysis in general is concerned, mainly two approaches can be found in literature: smeared crack analysis and discrete crack analysis. We consider here the second one. In this context embedded discontinuity elements have been proposed by Bolzon and Corigliano (2000), Wells and Sluys (2001), Oliver et al. (2001), Feist and Hofstetter (2006). Extended Finite Elements have been introduced by Moes and Belytschko (2002), a moving rosette in a fixed mesh was used by Wawrzynek and Ingraffea (1989) and a moving fracture in a fixed mesh by Camacho and Ortiz (1996).

We present a model for 3-D hydraulic fracturing based on a discrete fracture approach which uses remeshing in an unstructured mesh together with automatic mesh refinement. In our procedure the fracture follows the face of the elements around the fracture tip which is closest to the normal direction of the maximum principal stress at the fracture tip. The solution can be applied as it stands to realistic 3-D problems or be used as a benchmark problem for less precise methods such as the Particle Finite Element Method PFEM, introduced by Oñate et al. (2004). Oñate and Owen (2011).

The paper is organized as follows: in Sect. 2 we summarise briefly the governing equations and the cohesive fracture model adopted, in Sect. 3 we present the

remeshing strategy for an unstructured three-dimensional mesh, in Sect. 4 the adopted procedure for fracture advancement and in Sect. 5 one examples.

2 The mathematical model and its discretization

The porous medium is considered fully saturated throughout the domain. Also the fracture is filled with the same fluid. The derivation of the linear momentum balance equations and the mass balance equations for a fully saturated porous medium can be found in textbooks (Lewis and Schrefler 1989; Zienkiewicz et al. 1999) and is not repeated here. The mass balance equation for the fluid in the fracture (filler) is similar to that of the fluid in the pores. Simulation of fluid driven fracture propagation in a porous medium requires the introduction of appropriate constitutive relationships for the solid, and for the fluid defining the permeability within the crack and the rest of the domain. We will show in the sequel the weak form of the balance equations where the constitutive equations have been introduced.

2.1 Solid phase

In the framework of discrete crack models, the mechanical behaviour of the solid phase at a distance from the process zone is usually assumed as simple as possible. Let the complete domain be composed of a set of different homogeneous sub-domains. In the present formulation a Green-elastic or hyperelastic material is assumed for each component, being the mechanical behaviour dependent on effective stress as

$$\sigma'_{ij} = c_{ijrs} \varepsilon_{rs} \quad (1)$$

where the elastic coefficients depend on the strain energy function W and can be expressed in terms of Lamé constants as

$$c_{ijrs} = \frac{\partial^2 W}{\partial \varepsilon_{ij} \partial \varepsilon_{rs}} = \mu (\delta_{is} \delta_{jr} + \delta_{ir} \delta_{js}) + \lambda \delta_{ij} \delta_{rs} \delta_{ij} \quad (i, j, r, s = 1, 2, 3) \quad (2)$$

For the process zone we use the cohesive fracture model shown in Fig. 1 for sake of simplicity in a 2-D setting. The relations are however generalized for a 3-D situation as will be explained below. Between the real fracture apex which appears at macroscopic level and the apex of a fictitious fracture there is the process zone

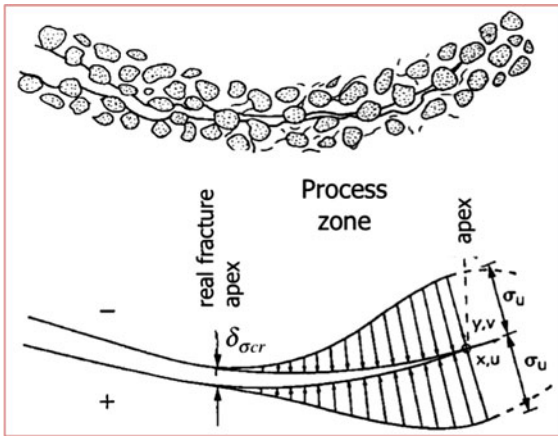


Fig. 1 Definition of cohesive crack geometry and model parameters

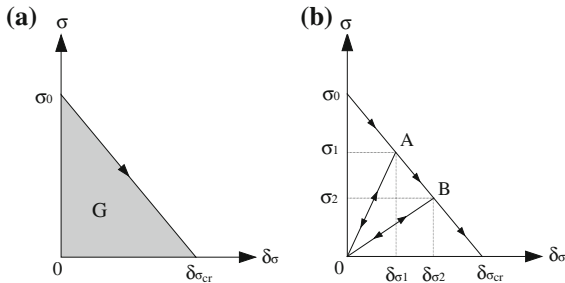


Fig. 2 Fracture energy (a) and loading/unloading law (b) for each homogeneous component

where cohesive forces act. A constitutive model links the cohesive forces to the crack opening in the process zone. In our approach the fracture is supposed to follow the side of the finite element in the apex zone which is closest to the normal to the plane with maximum tensile stress. Hence the following relations are valid for the side of the particular element considered in the apex. Clearly with propagating fracture this approach needs continuous updating of the mesh.

Within a generic component of the solid skeleton, a fracture can initiate or propagate under the assumption of mode I crack opening, provided that tangential relative displacements of the fracture lips are negligible. The cohesive forces are hence orthogonal to fractures planes. Following the [Barenblatt \(1959\)](#) and [Dugdale \(1960\)](#) model and accounting for [Hilleborg et al. \(1976\)](#), the cohesive law when opening monotonically increases is (Fig. 2)

$$\sigma = \sigma_0 \left(1 - \frac{\delta_{\sigma 1}}{\delta_{\sigma cr}} \right) \quad (3)$$

σ_0 being the maximum cohesive traction (closed crack), δ_{σ} the current relative displacement normal to the crack, $\delta_{\sigma cr}$ the maximum opening with exchange of cohesive tractions and $G = \sigma_0 \times \delta_{\sigma cr}/2$ the fracture energy. If after some opening $\delta_{\sigma 1} < \delta_{\sigma cr}$ the crack begins to close, tractions obey a linear unloading as

$$\sigma = \sigma_0 \left(1 - \frac{\delta_{\sigma 1}}{\delta_{\sigma cr}} \right) \frac{\delta_{\sigma}}{\delta_{\sigma 1}} \quad (4)$$

When the crack reopens, Eq. (4) is reversed until the opening $\delta_{\sigma 1}$ is recovered, then tractions obey again Eq. (3). The unloading path is also presented in Fig. 2. The individual homogeneous components differ only due to different values attributed to the fundamental parameters of Eqs. (3) and (4).

When tangential relative displacements of the sides of a fracture in the process zone can not be disregarded, mixed mode crack opening takes place. This is usually the case of a crack moving along an interface separating two solid components. In fact, whereas the crack path in a homogeneous medium is governed by the principal stress direction, the interface has an orientation that is usually different from the principal stress direction. The mixed cohesive mechanical model involves the simultaneous activation of normal and tangential displacement discontinuity and corresponding tractions. For the pure mode II, the model presented in Fig. 3 is referred to, where the relationship between tangential tractions and displacements is

$$\tau = \tau_0 \frac{\delta_{\sigma}}{\delta_{\sigma 1}} \frac{\delta_{\tau}}{|\delta_{\tau}|} \quad (5)$$

τ_0 being the maximum tangential stress (closed crack), δ_{τ} the relative displacement parallel to the crack and $\delta_{\sigma cr}$ the limiting value opening for stress transmission. The unloading/loading from/to some opening $\delta_{\sigma 1} < \delta_{\sigma cr}$ follow the same behaviour as for mode I and the traction law is

$$\tau = \tau_0 \left(1 - \frac{\delta_{\sigma 1}}{\delta_{\sigma cr}} \right) \frac{\delta_{\sigma}}{\delta_{\sigma 1}} \frac{\delta_{\tau}}{|\delta_{\tau}|} \quad (6)$$

which is valid for opening in the set $[0 < \delta_{\sigma 1} < \delta_{\sigma cr}]$, then the original path (Eq. 5) is followed. Figure 3 presents also the unloading/reloading relation.

For the mixed mode crack propagation, the interaction between the two cohesive mechanisms is treated as in [Camacho and Ortiz \(1996\)](#). By defining an equivalent or effective opening displacement δ and the scalar effective traction t as

$$\delta = \sqrt{\beta^2 \delta_{\tau}^2 + \delta_{\sigma}^2}, \quad t = \sqrt{\beta^{-2} t_{\tau}^2 + t_{\sigma}^2} \quad (7)$$

the resulting cohesive law is

Fig. 3 Fracture energy (a) and loading unloading law for the interface and mixed mode

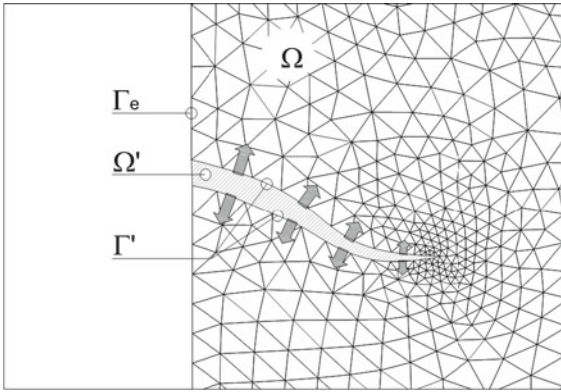
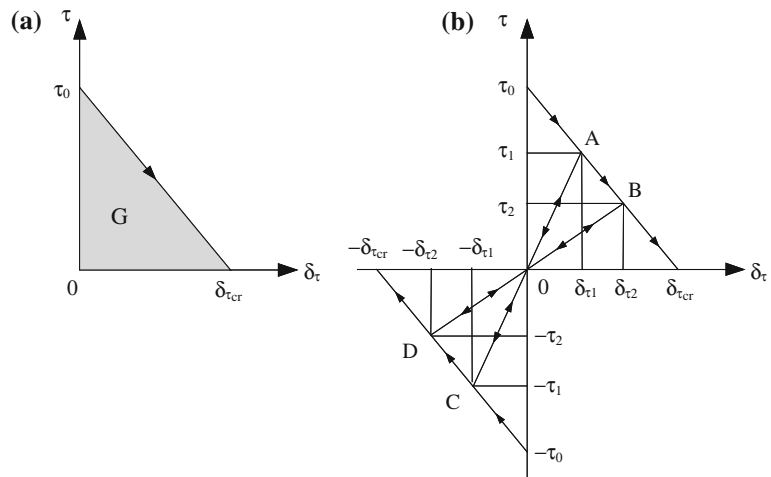


Fig. 4 Hydraulic crack domain

$$\mathbf{t} = \frac{t}{\delta} (\beta^2 \delta_\tau + \delta_\sigma) \tag{8}$$

β being a suitable material parameter that defines the ratio between the shear and the normal critical components. The cohesive law takes the same aspect as in Fig. 2, by replacing displacement and traction parameter with the corresponding effective ones.

Taking into account the cohesive forces, the effective stress principle and the symbols of Fig. 4, the linear momentum balance equation of the mixture is written as

$$\int_{\Omega} \delta \varepsilon_{ij} c_{ijrs} \varepsilon_{rs} d\Omega - \int_{\Omega} \delta \varepsilon_{ij} \bar{\alpha} \delta_{ij} p d\Omega - \int_{\Omega} \rho \delta u_i g_i d\Omega - \int_{\Gamma_e} \delta u_i t_i d\Gamma - \int_{\Gamma'} \delta u_i c_i d\Gamma' = 0 \tag{9}$$

where Ω is the domain of the initial boundary value problem, Γ_e is the external boundary and Γ' the bound-

ary of the fracture and process zone. $\delta \varepsilon_{ij}$ is the strain associated with virtual displacement δu_i , ρ the density of the mixture (solid plus fluid), g_i the gravity acceleration vector, t_i the traction on boundary Γ_e and c_i the cohesive tractions on the process zone as defined above. Traction and compressive values of the fluid pressure are taken as positive.

2.2 Liquid phase

Constant absolute permeability is assumed for the fluid fully saturated medium surrounding the fracture. As far as permeability within the crack is concerned, the validity of Poiseuille or cubic law is assumed. This has been stated for a long time in the case of laminar flow through open fractures and its validity has been confirmed in the case of closed fractures where the surfaces are in contact and the aperture decreases under applied stress. The cubic law has been found to be valid when the fracture surfaces are held open or are closed under stress, without significant changes when passing from opening to closing conditions. Permeability is not dependent on the rock type or stress history, but is defined by crack aperture only. Deviation from the ideal parallel surfaces conditions cause only an apparent reduction in flow and can be incorporated into the cubic law, which reads as (Witherspoon et al. 1980)

$$k_{ij} = \frac{1}{f} \frac{w^2}{12} \tag{10}$$

w being the fracture aperture and f a coefficient in the range 1.04–1.65 depending on the solid material. In the

following, this parameter will be assumed as constant and equal to 1.0. Incorporating the Poiseuille law into the weak form of water mass balance equation of the filler within the crack results in

$$\int_{\Omega'} \delta p \left\{ \frac{n}{K_w} \frac{\partial p}{\partial t} + \frac{\partial w}{\partial t} \right\} d\Omega' - \int_{\Omega'} (\delta p)_{,i} \left[\frac{w^2}{12\mu_w} (-p_{,j} + \rho_w g_j) \right] d\Omega' + \int_{\Gamma'} \delta p \bar{q}_w d\Gamma' = 0 \tag{11}$$

which represents the fluid flow equation along the fracture. It should be noted that the last term, representing the leakage flux into the surrounding porous medium across the fracture borders, is of paramount importance in hydraulic fracturing techniques. This term can be represented by means of Darcy’s law using the medium permeability and pressure gradient generated by the application of water pressure on the fracture lips. No particular simplifying hypotheses are hence necessary for this term. Equation (11) can be directly discretized by finite elements at the same stage as the other governing equations. Except for the compressibility term, this equation is also presented in (Boone and Ingraffea 1990), where it is discretized by the finite difference method and integrated separately along a predetermined path by using a staggered approach to obtain the pressure along the crack. Further, particular relationships for the leakage term have been introduced there, for instance impermeable boundaries. This staggered procedure resulted in a cumbersome method, requiring several thousand iterations, as the authors declare, due to the strong coupling of displacement and pressure fields, but, more importantly, it needs particular convergence and stability analyses (iteration convergence) to assess the numerical performance of the solution (Turska and Schrefler 1993). We solve this equation together with the other balance equations.

The mass balance equation for the pore water of the porous medium surrounding the fracture, becomes after incorporating Darcy’s law

$$\int_{\Omega} \delta p \left\{ \left(\frac{\bar{\alpha} - n}{K_s} + \frac{n}{K_w} \right) \frac{\partial p}{\partial t} + \alpha v_{i,i}^s \right\} d\Omega - \int_{\Omega} (\delta p)_{,i} \left[\frac{k_{ij}}{\mu_w} (-p_{,j} + \rho_w g_j) \right] d\Omega + \int_{\Gamma_c} \delta p q_w d\Gamma + \int_{\Gamma'} \delta p \bar{q}_w d\Gamma' = 0 \tag{12}$$

where δp is a continuous pressure distribution satisfying boundary conditions, n the porosity, K_w the bulk modulus for liquid phase, v_i^s the velocity vector of the solid phase, k_{ij} the permeability tensor of the medium, μ_w the dynamic viscosity of water, ρ_w its density and q_w the imposed flux on the external boundary. In the last term of Eq. (12) \bar{q}_w represents the water leakage flux along the fracture toward the surrounding medium. This term is defined along the entire fracture, i.e. the open part and the process zone.

It is worth mentioning that the topology of the domain Ω changes with the evolution of the fracture phenomenon. In particular, the fracture path, the position of the process zone and the cohesive forces are unknown and must be regarded as products of the mechanical analysis. The discretized governing equations which are shown next, are solved simultaneously to obtain the displacement and pressure fields together with the fracture path.

2.3 Discretized governing equations and solution procedure

Space discretization by means of the Finite Element Method of Equations (9) and (11, 12), adopting a vector notation and incorporating the constitutive equations, results in the following system of time differential equations (dot represents time derivative) at element level,

$$\begin{bmatrix} \mathbf{K}_E & -\mathbf{L}_E \\ -\mathbf{L}_E^T & \mathbf{S}_E \end{bmatrix} \begin{bmatrix} \dot{\mathbf{d}}_E \\ \dot{\mathbf{p}}_E \end{bmatrix} + \begin{bmatrix} \mathbf{0} & \mathbf{0} \\ \mathbf{0} & \mathbf{H}_E \end{bmatrix} \begin{bmatrix} \mathbf{d}_E \\ \mathbf{p}_E \end{bmatrix} = \begin{bmatrix} \dot{\mathbf{F}}_E \\ \mathbf{0} \end{bmatrix} + \begin{bmatrix} \mathbf{0} \\ \mathbf{G}_E \end{bmatrix} \tag{13}$$

We have taken advantage of the fact that Eqs. 11 and 12 have the same structure, hence only the parameters have to be changed in the appropriate element, depending whether they belong to the fracture or the surrounding porous medium. The submatrices in Eq. (13) are

$$\mathbf{K}_E^T = \int_{V_E} \mathbf{B}^T \mathbf{D} \mathbf{B} dV \tag{14a}$$

$$\mathbf{L}_E^T = \int_{V_E} \mathbf{N}^{pT} \left(\mathbf{m}^T - \frac{1}{3K_s} \mathbf{m}^T \mathbf{D} \right) \mathbf{B} dV \tag{14b}$$

$$\mathbf{S}_E = \int_{V_E} \mathbf{N}^{pT} \left(\frac{1-n}{K_s} + \frac{n}{K_f} - \frac{\mathbf{m}^T \mathbf{D} \mathbf{m}}{(3K_s)^2} \right) \mathbf{N}^p dV \tag{14c}$$

$$\mathbf{H}_E = \int_{V_E} (\nabla \mathbf{N}^p)^T \mathbf{K} \nabla \mathbf{N}^p dV \tag{14d}$$

$$\mathbf{G}_E = \int_{V_E} \mathbf{N}^{pT} q_E dV + \int_{\Gamma_{q,E}} \mathbf{N}^{pT} q_E^\Gamma d\Gamma + \sum \mathbf{N}^{pT} \mathbf{Q}^E \tag{14e}$$

$$\dot{\mathbf{F}}_E = \int_{V_E} \mathbf{N}^T \dot{\mathbf{f}}_E dV + \int_{\Gamma_E} \mathbf{N}^T \dot{\mathbf{t}}_E d\Gamma + \int_{\Gamma_{Ecrack}} \mathbf{N}^T \dot{c}_E d\Gamma \tag{14f}$$

where \mathbf{B} is the strain operator, \mathbf{D} the solid phase constitutive matrix, \mathbf{K} the permeability matrix, \mathbf{N} the matrix containing shape functions for the solid displacements and \mathbf{N}^p for the pressures, \mathbf{t}_E the vector of boundary tractions, \mathbf{f}_E the vector of body forces and $\mathbf{m} = [1 \ 1 \ 1 \ 0 \ 0]$. Formally the only change with respect to a fully coupled consolidation model (Lewis and Schrefler 1989) is given in Eq. (14f) where \dot{c}_E represents the cohesive traction rate and is different from zero only if the element has a side on the lips of the fracture Γ_{Ecrack} . Given that the liquid phase is continuous over the whole domain, leakage flux along the opened fracture lips is accounted for through Eq. (14d) together with the flux along the crack. Finite elements are in fact present along the crack, as shown in Fig. 4, which account only for the pressure field and have no mechanical stiffness. In the present formulation, non-linear terms arise through cohesive forces in the process zone and permeability along the fracture.

Global equations are assembled in usual way and can be integrated in time by means of the generalized trapezoidal rule. This yields the algebraic system of discretized equations, written for simplicity in a concise form as

$$\mathbf{A} \mathbf{x}_{n+1} = \mathbf{V}_n + \mathbf{Z}_{n+1} \tag{15}$$

being

$$\mathbf{x}_{n+1} = \begin{bmatrix} \mathbf{d} \\ \mathbf{p} \end{bmatrix}_{n+1}$$

$$\mathbf{A}_{n+1} = \begin{bmatrix} \mathbf{K} & -\mathbf{L} \\ -\mathbf{L}^T & \mathbf{S} + \alpha \Delta t \mathbf{H} \end{bmatrix}_{n+1}$$

$$\mathbf{V}_n = \begin{bmatrix} \mathbf{K} & -\mathbf{L} \\ -\mathbf{L}^T & \mathbf{S} - \Delta t (1 - \alpha) \mathbf{H} \end{bmatrix}_n \begin{bmatrix} \mathbf{d} \\ \mathbf{p} \end{bmatrix}_n$$

$$\mathbf{Z}_{n+1} = \begin{bmatrix} \mathbf{F} \\ \mathbf{0} \end{bmatrix}_{n+1} - \begin{bmatrix} \mathbf{F} \\ \mathbf{0} \end{bmatrix}_n + \Delta t (1 - \alpha) \begin{bmatrix} \mathbf{0} \\ \mathbf{G} \end{bmatrix}_n - \Delta t \alpha \begin{bmatrix} \mathbf{0} \\ \mathbf{G} \end{bmatrix}_{n+1} \tag{16}$$

n represents the time station and α the time discretization parameter. Implicit integration is used in the following applications ($\alpha = 0.5$).

3 3-D remeshing algorithm

As a consequence of the propagation of the cracks and ensuring evolution of the geometry an automatic 3-D remeshing technique is adopted. The starting point for the following developments is the numerical procedure for managing generic tetrahedral elements. In particular a modification of Quad-Edge structure proposed by Guibas and Stolfi (1985) is used for non-manifold surfaces (Weiler 1985, 1988). A useful survey on this subject and related implementation can be found in Campagna and Karbacher (2000). Modifications to an existing topological structure or new proposals are in any case possible, together with a definition of the pertinent Euler functions, also depending on the structure’s field of application. To create the finite element subdivisions, the *TMWEdge* data structure that simplifies the Quad-Edge and is similar to the Face-Edge suggested by Weiler (1985) is proposed here. This structure preserves the edge algebra and all mathematical and topological properties stated for the Quad-Edge formulation as well as efficiency in handling the adjacency of the Face-Edge. In addition it has been equipped with some new primitives directed to managing all the different meshing operations. The edge of the *TMWEdge* provides a cyclic list of the faces incident and allows moving from one triangle to the next one according to either a clockwise, or a counterclockwise order.

The choice of the data structure results from a compromise between computational and storage efficiency. In the *TMWEdge* structure the operations needed to construct an incremental Delaunay triangulation deal with creating, locating and deleting nodes, edges and triangles and require repetitive queries of neighbouring vertices, edges and polygons. These operation are implemented in the *TMWEdge* structure or obtained

Box 1 *TVertex* object

```

Tvertex{
    // Constructor (public)
    TVertex( double x, double y, double z);
    bool      IsEqual( double x, double y, double z, double toll);

    // Member Data (public)
    Tcoord*   pCoord;      // Vertex coordinates
    TEdge*    pEdge;       // Pointer to a connected edge
    TBoundary* pBoundary;  // Pointer to the geometric entities defining the boundary
                          //      (=0 for internal points)
}

```

Box 2 *TEdge* object

```

TEdge{
    //Constructor (public)
    // Attributes (public)
    TEdge*    Sym();
    TEdge*    O_Next();
    TEdge*    O_Prev();
    TEdge*    D_Next();
    TEdge*    D_Prev();
    TEdge*    L_Next();
    TEdge*    L_Prev();
    TEdge*    R_Next();
    TEdge*    R_Prev();

    TVertex*  Origin();
    TVertex*  Destination();

    TFace*    CwFace();
    TFace*    CcwFace();

    TVertex * pVertex;      // origin node (pointers to the global array)
    TFace*    pFace;        // first face following natural orientation
    int       Index;        // 0x01 : flag used to distinguish the position in TMWEdge
    . . . // other public methods
}

```

Box 3 *TMWEdge* structure

```

TMWEdge {
    // Constructor (public)
    TMWEdge();
    TMWEdge( TVertex* orgin, TVertex* dest );
    TEdge*   Edge();
    TEdge*   pEdge;
    . . . // other public methods
}

```

by the pertinent Euler functions. Geometrical information is preserved, hence the queries are performed in a limited time, almost independently of the number of elements in the list. For this reason, the topological structure also allows for a rapid execution of other operations such as swapping of edges, mesh quality control and similar tasks. Although not used in this paper,

the *TMWEdge* structure maintains the information for spatial operations (see Boxes 1, 2, 3, 4), in particular it is suitable for representing spatial surfaces and solids by means of triangles or polygonal surfaces of higher complexity and to deal with tetrahedral subdivisions. The usual topological transformations (translations, rotations, scaling) as well as more complex

Box 4 *TFace* object

```

TFace {
    //Constructor (public)
    TFace();
    TEdge& operator[] (int n);
    TVertex* operator() (int n);
    virtual int NumEdges() {return 3;}
    bool SetConnection ();
    bool AdjustConnections (TEdge* poldConn[]);

    // Member Data (protected)
    TEdge** pEdge; // array of edges
}

```

operations in space (such as sectioning of solids and their spatial visualisation) are also possible by adding a small amount of extra data.

The basic plane topological entities are vertices (*TVertex* object), edges (*TEdge* object) and faces (*TFace* object). Their union establishes the ordered complex *TMWEdge* structure.

The structure elements must fulfil some requirements which make their application possible and some conditions ensuing from the topological consistency:

- each element is required to reach, by means of internal pointers, its corresponding neighbouring entity;
- each edge can be shared by more than two faces (non-manifold);
- each edge must possess at least one face connected to it;
- each vertex must be connected to at least three edges;
- each face is defined by at least three vertices;
- there are no theoretical bounds to the number of edges connected to a vertex. This is a necessary requirement to obtain unstructured meshes.

Other information concerns the orientation. For each edge there is the possibility to define two orientations, the first, from the origin to the destination node (called *natural*) and the opposing one.

In an object-oriented framework, the *TVertex* class manages the node. It contains (Box 1) a *TCoord* object, which controls the coordinates, and a pointer to one of the edges connected to the vertex. The set of edges joined to each vertex forms the node *ring*.

The *TEdge* class contains and manages the information of each edge of the subdivision. The member data are (Box 2): *pVertex* pointer to the origin node, *pFace* pointer to the first face of the ring located at the left

of the edge when observing from *pVertex*, and *Index*, a short-type datum, i.e. a one byte char described in the following.

The three main entities (*TVertex*, *TMWEdge*, *TFace*) of the topological structure refer to 1, *n* or 3 *TEdge* objects respectively. In the first case, the pointer allows the object to know what and how many edges are linked to the vertex. Recognising whether the vertex belongs to the boundary of the domain without introducing new data is straightforward. The two pointers in *TMWEdge* establish an oriented edge and, finally, the three pointers in *TFace* describe the edges of the triangular element of the subdivision.

The efficiency of the structure increases if the *TEdge* object is able to recognise itself within the other entities in which it is contained. This means that each *TEdge* object has to know its position within the arrays containing it, and present in *TMWEdge* and *TFace*. The information contained in the *Index* datum is used for this purpose.

Depending on the way the edge operators are built, particularly for the function *Sym()* to be operative, it is necessary that operations which create the *TEdge* objects be exclusively performed in pairs of *TMWEdge* objects, by using dynamical memory allocation.

Box 2 lists the basic operators for the *TEdge* object. For instance *Sym()* yields the pointer to the edge having an opposite direction to the one under consideration. By using these operators the different entities necessary for meshing the domain are easily identified. E.g. it is possible to identify the vertex destination of edge *e*, which is represented by *e->Sym()->Origin()*, the vertex of the left triangle not shared by *e* is given by *e->D_Prev()->Origin()*.

The topological entities are completed by the structure *TFace*, which defines a face of the tessellation using *NumEdges()* edges suitably allocated in the

computer memory. The functions *SetConnection()* and *AdjustConnections()* (Box 4) initialise and modify data related to the incidences of the analysed and neighbour elements, respectively.

4 Fracture advancement

Because of the continuous variation of the domain as a consequence of the propagation of the cracks, also the boundary Γ' and the related mechanical conditions change. An extension to 3-D case of the procedure proposed by Schrefler et al. (2006) is adopted. Note that as compared to a 2-D situation the fracture tip becomes here a curve in space (front). Along the formed crack faces and in the process zone, boundary conditions are the direct result of the field equations. The adopted remeshing technique accounts for all these changes.

At each time station t_n , all the necessary spatial refinements are made, i.e. j successive front advancements are possible within the same time step (Fig. 5). If

a new node is created at the fracture advancement from the resulting elements for the filler are tetrahedral. If an internal node along the process zone advances, a new wedge element result in the filler.

The number of advancements in general depends on the chosen time step increment Δt , the adopted crack length increment Δs , and the variation of the applied loads. This requires continuous remeshing with a consequent transfer of nodal vector \mathbf{V}_m (Eq. 15) from the old to the continuously updated mesh (Fig. 6). Projection of this nodal vector between two consecutive meshes is obtained by using a suitable operator $\tilde{\mathbf{V}}_m(\Omega_{m+1}) = \aleph(\mathbf{V}_m(\Omega_m))$ (Secchi et al. 2007). The solution is then repeated with the quantities of mesh m but re-calculated on the new mesh $m + 1$ before advancing the crack tip to preserve as far as possible energy and momentum, see Fig. 6.

Fluid lag, i.e. negative fluid pressures at the crack tip which may arise if the speed with which the crack tip advances is sufficiently high so that for a given permeability water cannot flow in fast enough to fill the created space, can be obtained numerically only if an

Fig. 5 Multiple advancing fracture step at the same time station

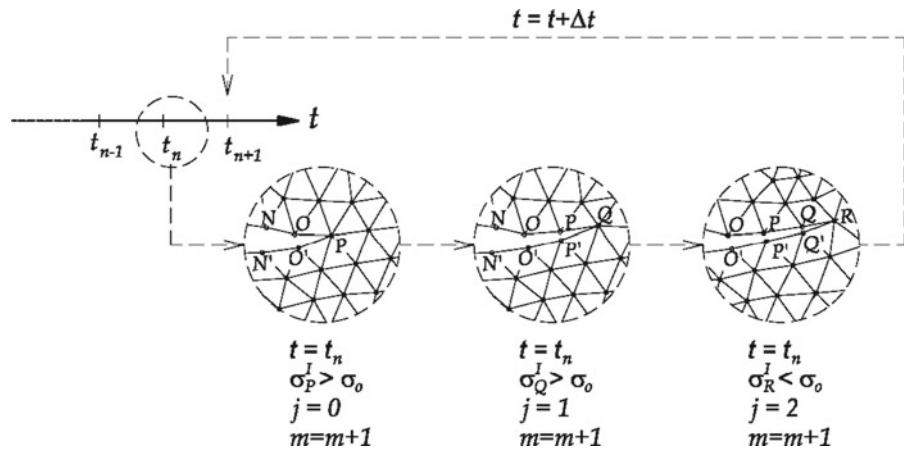


Fig. 6 Nodal forces projection algorithm. **a** Nodal forces at time station n on mesh m . **b** Nodal forces of time station n on mesh $m + 1$ before projection. **c** Nodal forces of time n on mesh $m + 1$ referred to nodes of the latter

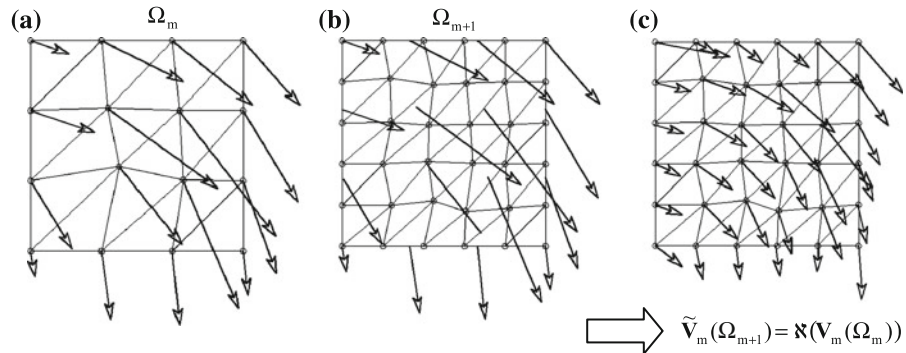


Fig. 7 Problem geometry for ICOLD benchmark and calculated crack path with 2-D analysis

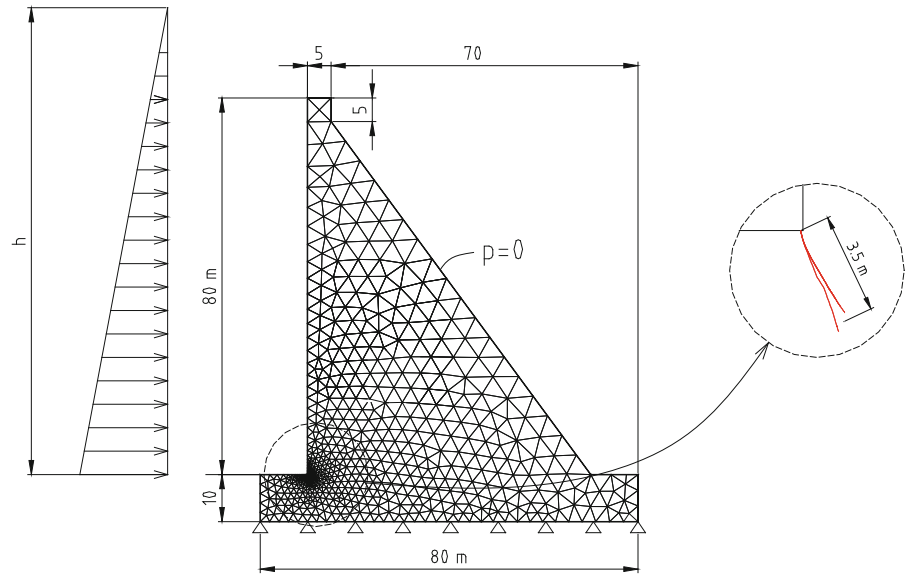
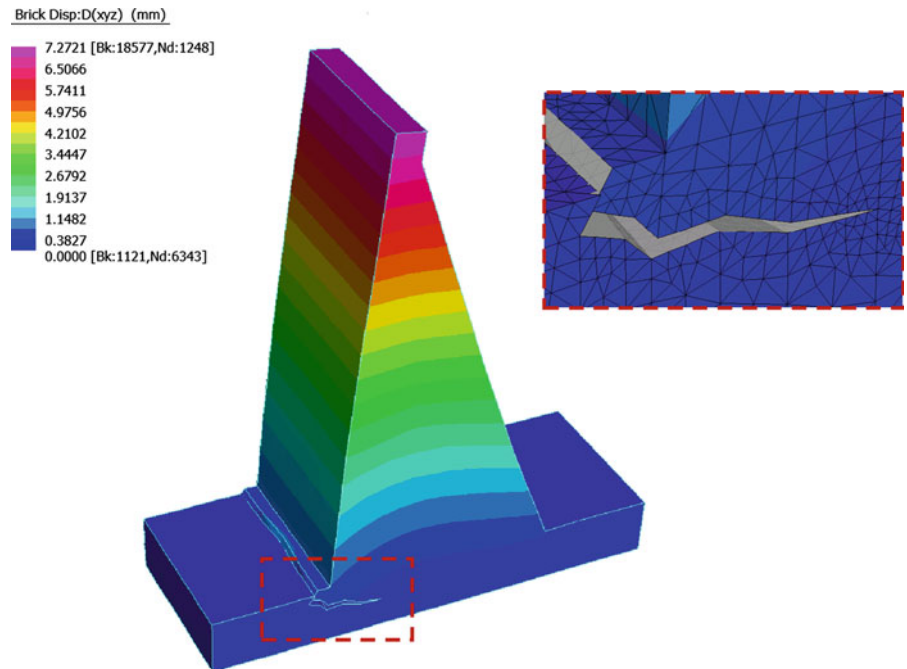


Fig. 8 Fracture at the base of the dam

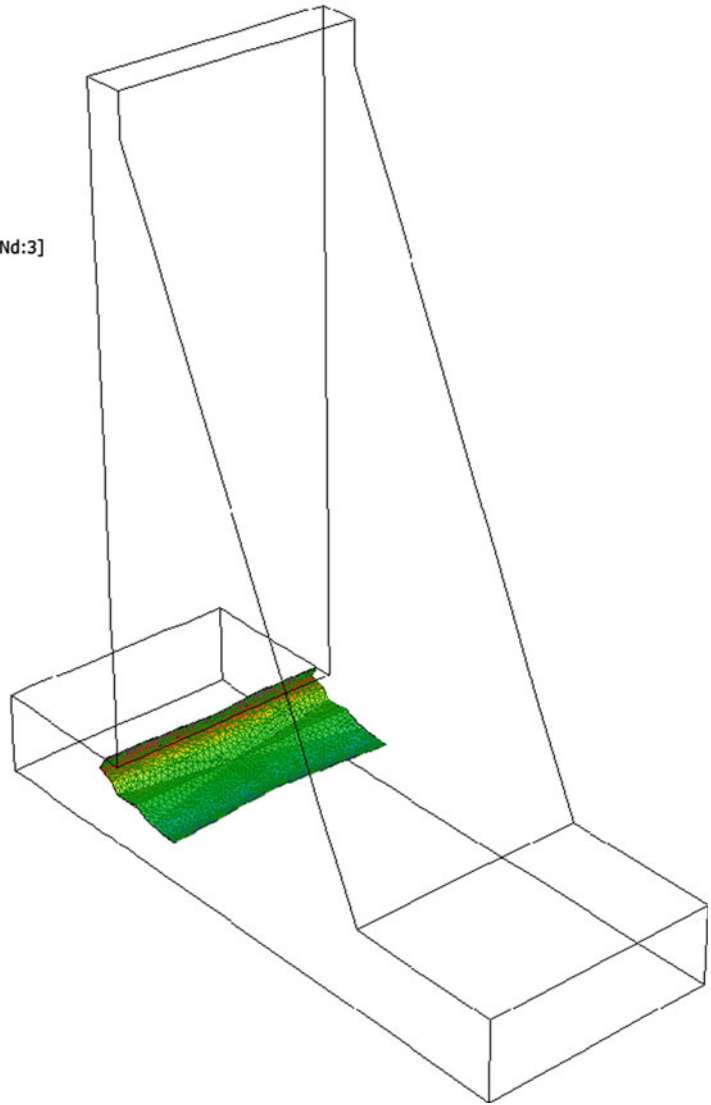
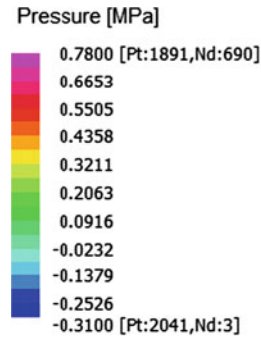


element threshold number is satisfied over the process zone. This number is given by the ratio of elements over process zone and can be estimated in advance from the problem at hand and the expected process zone length. Hence a sort of object oriented refinement is needed locally (Secchi et al. 2008).

5 Example

The 3-D code has been validated with respect to consolidation problems (Secchi et al. 2008).

The following application deals with a benchmark proposed by ICOLD. The benchmark consists

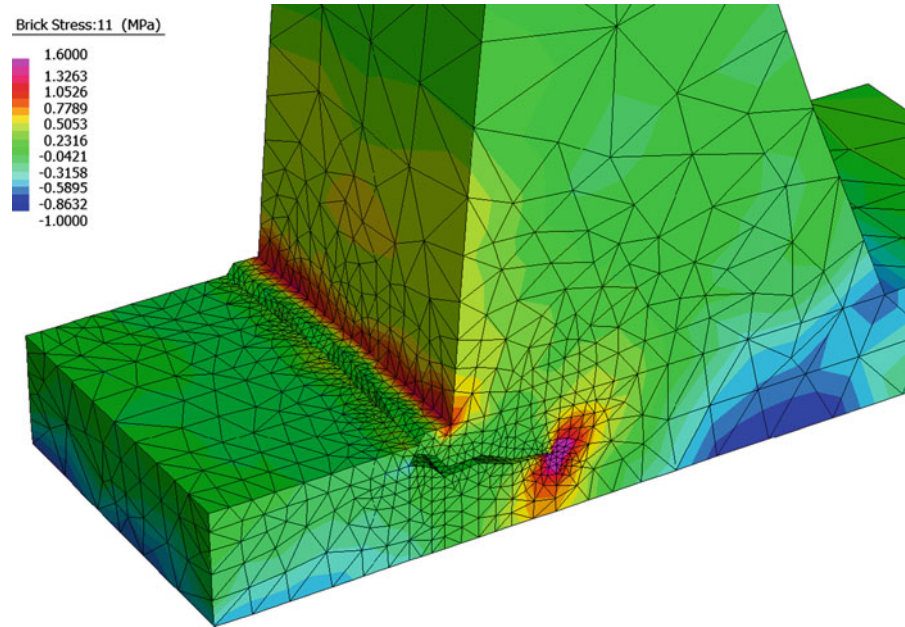
Fig. 9 Pressure field inside the 'filler'

in the evaluation of failure conditions as a consequence of an overtopping wave acting on a concrete gravity dam. The geometry of the dam is shown in Fig. 7 together with initial and boundary conditions and an intermediate discretization. Differently from the original benchmark, the dam concrete foundation is also considered, which has been assumed homogeneous with the dam body. In such a situation, the crack path is unknown. On the contrary, when a rock foundation is present, the crack naturally develops at the interface between dam and foundation.

As far as initial conditions for water pressure are concerned, it is assumed that during building operations and before filling up the reservoir, pressure can dissipate in all the dam body. As consequence zero initial pore pressure is assumed in the simulation. A more realistic assumption is the hypothesis of partial saturation of the concrete, which would require a further extension of the present mathematical model.

Applied loads are the dam self-weight and the hydrostatic pressure due to water in the reservoir growing from zero to the overtopping level h (which is higher than the dam). The material data for the concrete are

Fig. 10 Principal stress map-contour



those assigned in the benchmark, whereas for permeability the value of 10^{-12} cm/s has been assumed. This value could suggest the hypothesis of an impermeable material. This limit case can be analysed by the present model locating the diffusion phenomenon in restricted areas near the wetted side of the dam and along the crack sides. Such a condition is easily handled by the used mesh generator, but has not been applied in the following. The proper representation of the cohesive forces requires a fine mesh in the area of the process zone. This is shown in Fig. 8, which represents the process zone when the fracture length is about 15 m and corresponds to an intermediate step of the analysis when the water level is 80 m. The pressure distribution inside the fracture is shown in Fig. 9 and the contour of principal stresses in Fig. 10.

This problem has been solved as a 2-D case in Schrefler et al. (2006). The nucleation point of the fracture and the inclination of about 80° during the first 5 m of the fracture are similar in both solutions. During further advancement steps the inclination of the 3-D solution diminishes also as a consequence of the boundary conditions at the base. At the crack tip after each advancement appears a fluid lag as in the 2-D case. The negative pressures diminish rapidly once the fracture is stabilized within the considered time step because of the inflow of water. The 3-D and 2-D solutions give comparable stress and pressure distributions being the plane-

strain model representative of the 3-D case; in fact this problem has been chosen for validation purposes. The general 3-D space-adaptive procedure involves a higher number of dofs of the corresponding plain strain model and requires, therefore, a higher computational effort to obtain mesh-independent solutions. In many engineering situations 3-D analysis is compulsory.

6 Conclusion

Some important conclusions can be drawn from this application:

- the mechanical behaviour of the solid skeleton strongly depends on the characteristic permeability of the fluid within the crack. Crack paths are in fact different, as result of the different stress fields;
- the crack path cannot be forecast; hence the traditional use of special/interface elements to simulate fracture propagation in large structures is prevented. One alternative to the successive remeshing is the use of cumbersome discretizations of the areas interested by fracture, but also this strategy is not viable in the case of dams. Further, the used technique for the analysis of the nucleation of the fracture does not require the presence of an initial notch and requires a very limited amount of

information to be initially defined. Another alternative would be the use of X-Fem, but there are only few 3-D applications around (Moes et al. 2002; Gravouil et al. 2002; Sukumar et al. 2008); none of them addresses hydraulic fracturing.

- numerical results show a mesh-size dependence that can be only reduced with the adaptivity in space considered in the analysis. A full elimination would require also adaptivity in time which was investigated in (Secchi et al. 2008) using a time discontinuous Galerkin method;
- trial simulations have shown that results depend on the presence of the ‘filler’ inside the crack. In particular a different crack surface path and a different fracture propagation velocity has been obtained with and without filler.

Acknowledgements Partial support was provided by the Strategic Research Project “Algorithms and Architectures for Computational Science and Engineering”—AACSE (STPD08JA32—2008) of the University of Padova (Italy)

References

- Advani SH, Lee TS, Dean RH, Pak CK, Avasthi JM (1997) Consequences of fluid lag in three-dimensional hydraulic fractures. *Int J Numer Anal Methods Geomech* 21:229–240
- Barenblatt GI (1959) The formation of equilibrium cracks during brittle fracture: general ideas and hypotheses. Axially-symmetric cracks. *J Appl Math Mech* 23:622–636
- Bolzon G, Corigliano A (2000) Finite elements with embedded displacement discontinuity: a generalized variable formulation. *Int J Numer Methods Eng* 49:1227–1266
- Boone TJ, Ingraffea AR (1990) A Numerical Procedure for Simulation of hydraulically driven fracture propagation in poroelastic media. *Int J Numer Anal Methods Geomech* 14:27–47
- Camacho GT, Ortiz M (1996) Computational modelling of impact damage in brittle materials. *Int J Solids Struct* 33:2899–2938
- Campagna S, Karbacher S (2000) Polygon meshes. In: Girod B, Greiner G, Niemann N (eds) *Principles of 3D image analysis and synthesis*. Kluwer Academic Publisher, Boston pp 142–152
- Carter BJ, Desroches J, Ingraffea AR, Wawrzynek PA (2000) Simulating fully 3-D hydraulic fracturing. In: Zaman, Booker and Gioda (eds) *Modeling in geomechanics*. Wiley, Chichester, pp 525–567
- Cleary MP (1978) Moving singularities in elasto-diffusive solids with applications to fracture propagation. *Int J Solids Struct* 14:81–97
- Detournay E, Cheng AH (1991) Plane strain analysis of a stationary hydraulic fracture in a poroelastic medium. *Int J Solids Struct* 27:1645–1662
- Dugdale DS (1960) Yielding of steel sheets containing slits. *J Mech Phys Solids* 8:100–104
- Feist C, Hofstetter G (2006) An embedded strong discontinuity model for cracking of plain concrete. *Comput Methods Appl Mech Eng* 195(52):7115–7138
- Garagash D, Detournay E (2000) The tip region of a fluid-driven fracture in an elastic medium. *J Appl Mech* 67:183–192
- Guibas LJ, Stolfi J (1985) Primitives for the manipulation of general subdivisions and the computation of Voronoi diagrams. *ACM Trans Graph* 4:74–123
- Gravouil A, Moes N, Belytschko T (2002) Non-planar 3D crack growth by the extended finite element and level sets-part II: level set update. *Int J Numer Methods Eng* 53:2569–2586
- Hilleborg A, Modeer M, Petersson PE (1976) Analysis of crack formation and crack growth in concrete by means of fracture mechanics and finite elements. *Cem Concret Res* 6:773–782
- Huang NC, Russel SG (1985a) Hydraulic fracturing of a saturated porous medium—I: general theory. *Theor Appl Fract Mech* 4:201–213
- Huang NC, Russel SG (1985b) Hydraulic fracturing of a saturated porous medium—II: special cases. *Theor Appl Fract Mech* 4:215–222
- ICOLD (1999) Fifth international benchmark workshop on numerical analysis of dams, Theme A2, Denver, Colorado
- Lewis RW, Schrefler BA (1989) *The finite element method in the static and dynamic deformation and consolidation in porous media*. Wiley, Chichester
- Moes N, Belytschko T (2002) Extended finite element method for cohesive crack growth. *Eng Fract Mech* 69(7):813–833
- Moes N, Gravouil A, Belytschko T (2002) Non-planar 3D crack growth by the extended finite element and level sets-Part I: mechanical model. *Int J Numer Methods Eng* 53:2549–2568
- Oliver J, Huespe AE, Pulido MDG, Chaves E (2001) From continuum mechanics to fracture mechanics: the strong discontinuity approach. *Eng Fract Mech* 69(2):113–136
- Oñate E, Owen R (eds) (2011) *Particle-based methods*. Springer, New York
- Oñate E, Idelsohn SR, Del Pin F, Aubry R (2004) The particle finite element method. An overview. *Int J Comput Methods* 1(2):267–307
- Perkins TK, Kern LR (1961) Widths of hydraulic fractures. *SPE J* 222:937–949
- Réthoré J, Borst Rde, Abellan MA (2008) A two-scale model for fluid flow in an unsaturated porous medium with cohesive cracks. *Comput Mech* 42:227–238
- Rice JR, Cleary MP (1976) Some basic stress diffusion solutions for fluid saturated elastic porous media with compressible constituents. *Rev Geophys Space Phys* 14:227–241
- Schrefler BA, Secchi S, Simoni L (2006) On adaptive refinement techniques in multifield problems including cohesive fracture. *CMAME* 195:444–461
- Secchi S, Simoni L (2003) An Improved Procedure for 2-D unstructured Delaunay mesh generation. *Adv Eng Softw* 34:217–234
- Secchi S, Simoni L, Schrefler BA (2007) Numerical procedure for discrete fracture propagation in porous materials. *Int J Numer Anal Methods Geomech* 31:331–345
- Secchi S, Simoni L, Schrefler BA (2008) Numerical difficulties and computational procedures for thermo-hydro-mechani-

- cal coupled problems of saturated porous media. *Comput Mech* 43:179–189
- Sukumar N, Chopp DL, Bechet E, Moes N (2008) Three dimensional non-planar crack growth by a coupled extended finite element and fast marching method. *Int J Numer Methods Eng* 76:727–748
- TAMEST (2011) The Academy of Medicine, Engineering & Science of Texas, Texas Energy Summit, Executive Summary, Austin, Texas 78701
- Turska E, Schrefler BA (1993) On convergence conditions of partitioned solution procedures for consolidation problems. *Comput Methods Appl Mech Eng* 106:51–63
- Wawrzynek PA, Ingraffea AR (1989) An interactive approach to local remeshing around a propagating crack. *Finite Elem Anal Design* 5(1):87–96
- Weiler K (1985) Edge-based data structures for solid modeling in curved surface environments. *IEEE Comput Graph Appl* 5(1): 21–40
- Weiler K (1988) The radial-edge structure: a topological representation for non-manifold geometric boundary representation. In: Wozny MJ, McLaughlin HW, Encarnacao JL (eds) *Geometric modeling for CAD applications*. North Holland, New York, pp 3–36
- Wells GN, Sluys LJ (2001) Three-dimensional embedded discontinuity model for brittle fracture. *Int J Solids Struct* 38(5):897–913
- Witherspoon PA, Wang JSY, Iwai K, Gale JE (1980) Validity of Cubic law for fluid flow in a deformable rock fracture. *Water Resour Res* 16:1016–1024
- Zhu JZ, Zienkiewicz OC (1988) Adaptive techniques in the finite element method. *Commun Appl Numer Methods* 4:197–204
- Zienkiewicz OC, Chan A, Pastor M, Schrefler BA, Shiomi T (1999) *Computational geomechanics with special reference to earthquake engineering*. Wiley, Chichester